Catalysis Science & Technology

Ethylene Polymerization with a Crystallographically Well-Defined Metal–Organic Framework Supported Catalyst

Journal:	*Catalysis Science & Technology*
Manuscript ID	CY-ART-11-2021-001990.R1
Article Type:	Paper
Date Submitted by the Author:	20-Dec-2021
Complete List of Authors:	Goetjen, Timothy; Northwestern University, Department of Chemistry Knapp, Julia; Northwestern University, Chemistry Syed, Zoha; Northwestern University, Chemistry; Argonne National Laboratory, Chemical Sciences and Engineering Hackler, Ryan; Argonne National Laboratory, Chemical Sciences and Engineering Division Zhang, Xuan; Northwestern University, Delferro, Massimiliano; Argonne National Laboratory, Chemical Sciences and Engineering Division Hupp, Joseph; Northwestern University, Chemistry Farha, Omar; Northwestern University, Department of Chemistry; Northwestern University, Chemical and Biological Engineering

ARTICLE

Ethylene Polymerization with a Crystallographically Well-Defined Metal–Organic Framework Supported Catalyst

Received 00th January 20xx,
Accepted 00th January 20xx

DOI: 10.1039/x0xx00000x

Timothy A. Goetjen,[a] Julia G. Knapp,[a] Zoha H. Syed,[a,b] Ryan A. Hackler,[b] Xuan Zhang,[a] Massimiliano Delferro,[b] Joseph T. Hupp,[a*] Omar K. Farha[a,c*]

The inherent crystallinity of metal–organic framework (MOF) catalysts offers the possibility to understand the structure of the active site at the molecular level. This property is often lacking in traditional amorphous supports. Cr-SIM-NU-1000, a MOF-supported Cr^{3+} heterogeneous catalyst, is shown to be competent for ethylene polymerization after activation with $AlEt_2Cl$ (DEAC), producing crystalline linear polyethylene (PE). The polymer produced has a low polydispersity ($Đ$ = 2.0), in marked contrast to the Phillips supported chromium catalyst, Cr@SiO_2 ($Đ$ ~ 8-65). Cr-SIM-NU-1000 achieves a turnover frequency of 2.6 x 10^3 h^{-1} under 40 bar ethylene pressure at room temperature, with corresponding PE productivity of 1.3 x 10^5 g PE mol^{-1} Cr h^{-1}. Single crystal X-ray diffraction (SC-XRD) of the pre-catalyst was conducted by collecting a structure of alkyl aluminum (DEAC) co-catalyst treated Cr-SIM-NU-1000. This crystal structure provides insight into the interactions between DEAC co-catalyst and Cr active site, revealing a Cr-C bond after treatment with DEAC. Furthermore, DEAC is crystallographically resolved at the terminal oxy-ligands of the node and likely also exists within the window pores of the framework between nodes, based on electron density mapping. Cr-SIM-NU-1000 offers the opportunity to study a structurally well-defined olefin polymerization system, with atomically precise characterization of the pre-catalyst structure. This allows the proposal of a mechanism and feeds into future development of next-generation heterogeneous catalyst systems.

Introduction

Polymers play an integral role in today's society.[1] Efficient and selective synthesis of these polymers, especially of polyethylene (PE) for which there are hundreds of specialized grades, is essential for the economical manufacturing of desired products.[2] To achieve this, heterogeneous catalysts are desired to enhance the activity and selectivity of these transformations (**Scheme 1**).[3] In the realm of olefin polymerization, a canonical example of a successful industrial heterogeneous catalyst is the Phillips catalyst (Cr@SiO_2), which is responsible for approximately 50% of global polyethylene production.[2, 4] While this is an efficacious demonstration of industrial heterogeneous catalysis, structural understanding and derivation of structure-activity relationships remain elusive.[5]

There is widespread debate on the nature of the pre-catalyst species and active site(s) of systems such as the Phillips catalyst.[6] While non-diffractive spectroscopic techniques aim to elucidate the pre-catalyst structure and nature of the active site(s),[7] and provide some mechanistic insight,[4] a comprehensive understanding through these methods is nontrivial.[6] The need for atomically precise insight into structure is evidenced by the drastic effect variations in catalyst structure have on activity and product selectivity.[8, 9] Therefore, to better understand the influence of structure on polymer properties, an analogous crystalline support can be envisioned, affording numerous additional characterization techniques for probing catalyst speciation.

Scheme 1

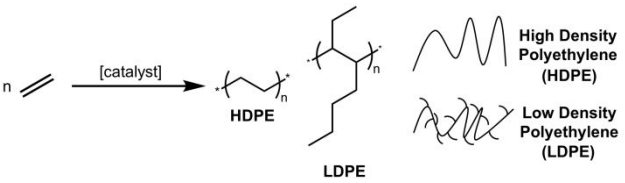

Ethylene polymerization reaction aided by a heterogeneous catalyst with examples of polymers. Visual representation of polymers shows the contrast between minimal to no branching (HDPE) and substantial branching (LDPE) in the two example types.

Metal–organic frameworks (MOFs) are a highly tunable class of porous materials, comprised of inorganic nodes (metal ions, clusters, etc.) and multi-topic organic linkers (carboxylates, phosphonates, pyridines, etc.).[10] Due to the modularity of their structures and functions,[11-16] MOFs have proven useful for a wide suite of potential applications[17] including gas separations and storage,[18-20] chemical sensing,[21, 22] water purification,[23, 24] and catalysis.[25-30] Among these applications, catalysis has largely capitalized upon the tailorable nature of MOFs to enhance activity and selectivity across various transformations.[31-38] Notably, MOFs are crystalline and thus can be characterized *via* single crystal X-ray diffraction (SC-XRD), even after

[a] *Department of Chemistry and International Institute of Nanotechnology, Northwestern University, 2145 Sheridan Road, Evanston, IL, USA 60208.*
[b] *Chemical Sciences and Engineering Division, Argonne National Laboratory, 9700 South Cass Avenue, Lemont, IL, USA 60439.*
[c] *Department of Chemical and Biological Engineering, Northwestern University,2145 Sheridan Road, Evanston, IL, USA 60208.*

Electronic Supplementary Information (ESI) available: [Additional catalysis, characterization, and crystallographic data (PDF). Crystallographic information file of DEAC@Cr-SIM-NU-1000 (CIF) deposited to the CCDC - Deposition #2115104]. See DOI: 10.1039/x0xx00000x

post-synthetic modification.[39-45] This allows MOFs to be used as crystalline analogues capable of yielding information that is complementary to what can be learned structurally by anchoring catalysts on traditional materials such as amorphous oxides including silica, alumina, and zirconia.[46]

Zr-based MOFs, in particular, are desirable as catalyst supports due to high chemical and thermal stabilities, as well as providing uniform and spatially isolated catalyst deposition sites.[12, 47] In particular, NU-1000 ($[Zr_6(\mu_3\text{-}O)_4(\mu_3\text{-}OH)_4(OH)_4(OH_2)_4](TBAPy)_2$, $TBAPy^{4-}$ = 1,3,6,8-tetrakis(p-benzoate)pyrene, NU = Northwestern University),[48] comprised of Zr_6 nodes and pyrene-based tetratopic carboxylate linkers, offers terminal hydroxyl and aqua groups as grafting sites.[49]

Herein, we demonstrate the activity of a MOF-supported Cr catalyst, Cr-SIM-NU-1000, for ethylene polymerization. Upon exposure to pure (99.9%) ethylene at room temperature with diethylaluminum chloride (DEAC) as a co-catalyst (for structure see **Figure S1**), Cr-SIM-NU-1000 yields crystalline, linear polyethylene. Ethylene polymerization activity of Cr-SIM-NU-1000 was screened across a range of ethylene pressures (5 – 40 bar), and polymer samples were characterized by gel permeation chromatography (GPC), differential scanning calorimetry (DSC), solution-phase ^1H and ^{13}C nuclear magnetic resonance (NMR) spectroscopy, and solid-state ^{13}C Cross Polarization/Magic Angle Spinning (CP/MAS) NMR spectroscopy. Applying to macroscopic single crystals of Cr-SIM-NU-1000 the same co-catalyst treatment as that for the microcrystalline powders used here for catalysis experiments, affords DEAC@Cr-SIM-NU-1000 single crystals. SC-XRD analysis reveals that the alkyl aluminum co-catalyst is sited on the MOF node and directed into the void space (or "c-pore") that cross-connects triangular and hexagonal channels.

Previously considered as an ethylene oligomerization catalyst,[50] Cr-modified NU-1000, called Cr-SIM-NU-1000, showed activity implying that the catalyst could efficiently polymerize ethylene under different catalytic conditions. Furthermore, the reported single crystal structure of Cr-SIM-NU-1000 revealed siting of the catalyst upon the Zr_6 nodes of the MOF support, providing an opportunity to probe the reactivity of a Cr-based ethylene polymerization catalyst with a known uniform structure (**Figure 1**),[50] and propose a plausible mechanism.

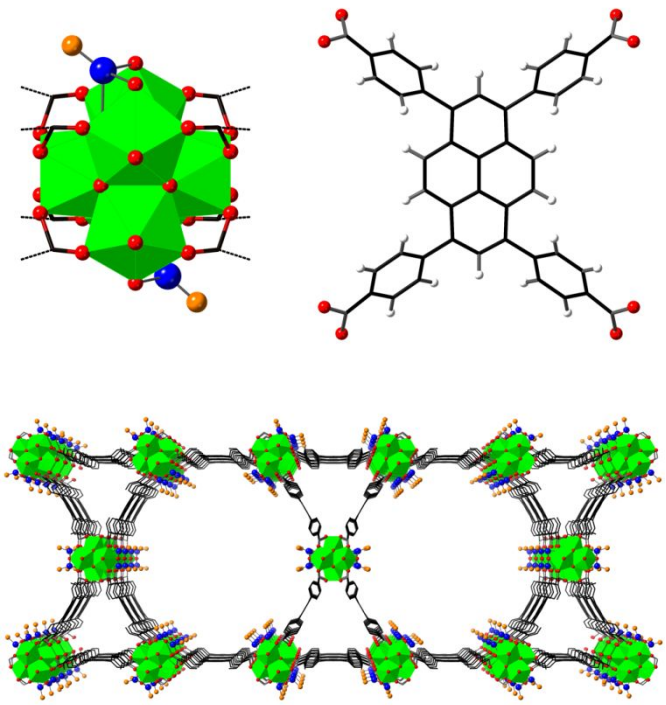

Figure 1. Visual representation of Cr-SIM-NU-1000 from experimental crystal structure.[50] Node (top right) and linker (top left) components, and overall structure of Cr-SIM-NU-1000 (bottom). Cr shown at the node in two of four crystallographically equivalent sites with 0.25 occupancy, while the MOF structure shows all four sites. Atom colors: H (white), C (black), O (red), Cl (orange), Cr (blue), and Zr (green). Hydrogens omitted from node and MOF structure for clarity.

Experimental

Materials and Methods

Acetone, *N,N*-dimethylformamide (DMF), hydrochloric acid were purchased from Fisher Scientific (Waltham, MA) and used as received. Benzoic acid, trifluoroacetic acid (TFA), zirconyl chloride octahydrate, chromium(II) chloride (99.99% trace metals), and 1.0 M diethylaluminum chloride (DEAC) in heptane were purchased from Sigma-Aldrich (St. Louis, MO) and used as received. ***Caution diethylaluminum chloride is pyrophoric and should only be handled under an inert atmosphere and with care***. Anhydrous heptane was purchased from Sigma-Aldrich and further dried by soaking over 3 Å molecular sieves. *N,N*-diethylformamide (DEF) was purchased from TCI America (Portland, OR) and used as received. UHP N_2 (99.999%), UHP Ar (99.999%), and UHP ethylene (99.9%) were purchased from Airgas (Radnor, PA) and used as received. 1,3,6,8-tetrakis(p-benzoic acid)pyrene (H_4TBAPy) was synthesized based on literature procedure.[48]

NU-1000 Powder Synthesis. 1,3,5,8-tetrakis(p-benzoic acid)pyrene, was synthesized according to reported procedure.[48] NU-1000 was synthesized, acid activated, and washed according to previously published procedures.[48, 51]

Cr-SIM-NU-1000 Powder Synthesis. Cr-SIM-NU-1000 was prepared by previously reported procedure.[50] Cr-SIM-NU-1000 was prepared by mixing 200 mg NU-1000 into 25 mL of a 0.1 M $CrCl_2$ solution in *N,N*-dimethylformamide (DMF) and heated overnight at 100 °C. The sample was washed with fresh DMF (3 x 40 mL). Then the sample was washed with acetone (3 x 40 mL) to exchange the solvent to remove DMF and left to soak overnight in fresh acetone. The sample was dried at 80 °C in a vacuum oven for 2 hours, and then thermally activated at 120 °C under dynamic vacuum on a Smart VacPrep for 16 hours.

DEAC@Cr-SIM-NU-1000 Powder Synthesis. Freshly DMF washed Cr-SIM-NU-1000 powder was solvent exchanged to acetone by washing 3 times and then soaking overnight. Then, after decanting the acetone, the powder was placed in a vacuum oven at 80 °C for 3 hours. Then, it was thermally activated at 120 °C under dynamic vacuum on a Smart VacPrep for 16 hours. The powder was then transferred into an Ar filled glovebox. Next, it was soaked in anhydrous heptane before decanting the solvent and exposing the powder to 1.0 M diethylaluminum chloride in heptane consistent with the catalysis experiments. After 1 h, the solvent was decanted and exchanged for fresh heptane 3 times with a 30 min. soaking period in between. The solvent was then exchanged to pentane, where the powder was allowed to soak for a total of 1.5 h during which 3 washes and subsequent soaks were performed. After

decanting as much pentane as possible, the powder was held under dynamic vacuum on a Smart VacPrep for 16 hours.

Ethylene Polymerization. In an Ar filled glovebox, 10 mg Cr-SIM-NU-1000, 5 mL anhydrous heptane, and 1.0 mL of diethylaluminum chloride (1.0 M in heptane) were charged into a 50 mL 4590 micro bench top autoclave Parr reactor. The reactor was then sealed, transferred out of the glovebox and connected to the gas inlet, pressure gauge, and thermocouple at the reactor station. The reactor was then set to stir at 200 rpm and pressurized to between 5 and 40 bar with C_2H_4. After 1 hour, the reaction was vented and opened, after which the solid polymer was recovered for analysis.

Analytical Measurements. Powder X-ray diffraction (PXRD) data was collected at the IMSERC X-ray Facility at Northwestern University on a STOE-STADI-P powder diffractometer equipped with an asymmetric curved Germanium monochromator (CuKα1 radiation, λ = 1.54056 Å) and one-dimensional silicon strip detector (MYTHEN2 1K from DECTRIS). The line focused Cu X-ray tube was operated at 40 kV and 40 mA. Powder was packed in a 3 mm metallic mask and sandwiched between two layers of polyimide tape. Intensity data from 1 to 40 degrees 2θ were collected over a period of 5 mins.

N_2 adsorption isotherms were measured on a Micromeritics Tristar II 3020 (Micromeritics, Norcross, GA) at 77 K with 30-80 mg pre-activated sample at 120 °C for 16 h under high vacuum using a Smart VacPrep (Micromeritics, Norcross, GA). BET area was calculated in the region P/P_0 = 0.005-0.05 and pore-size distributions were obtained *via* density functional theory (DFT) calculations using a carbon slit-pore model with a N_2 kernel.

Inductively coupled plasma optical-emission spectroscopy (ICP-OES) was performed at the QBIC facility at Northwestern University on a Thermo iCAP 7600 Spectrometer (ThermoFisher, Waltham, MA). In each preparation, ~3 mg samples were digested in 2 mL concentrated nitric acid in a 2-5 mL Biotage (Uppsala, Sweden) microwave vial. Biotage SPX microwave reactor (software version 2.3, build 6250) was used to heat the mixture to 150 °C for 15 min. 300 µL of the digested sample was removed and diluted to 10 mL with ultrapure Millipore water.

Supercritical CO_2 drying was performed using a Tousimis Samdri-PVT-3D supercritical CO_2 drier, exchanging ethanol for supercritical CO_2 five times with a minimum soaking time of 1 h between exchanges. The temperature was then increased to the supercritical point and the instrument pressure was bled at 0.5 cm^3/min.

Single-crystal X-ray diffraction (SC-XRD) intensity data of a yellow-green rod crystal were collected at 200 K. A suitable single crystal was mounted on a MiTeGen loop with paratone oil on an XtaLAB Synergy diffractometer equipped with a micro-focus sealed X-ray tube PhotonJet (Cu) X-ray source and a Hybrid Pixel Array Detector(HyPix) detector. Temperature of the crystal was controlled with an Oxford Cryosystems low-temperature device. Data reduction was performed with the CrysAlisPro software using an empirical absorption correction. The structure was solved with the ShelXT structure solution program using the Intrinsic Phasing solution method and by using Olex2 as the graphical interface. The model was refined with ShelXL using least squares minimization. The CIF has been deposited in the Cambridge Crystallography Data Centre under Deposition #2115104 and is freely accessible at https://www.ccdc.cam.ac.uk/.

Scanning electron microscopy (SEM) images were collected at Northwestern University's EPIC/NUANCE facility using an FEI Quanta 650 ESEM microscope. All samples were coated with 9 nm OsO_4 before imaging.

Gel permeation chromatography (GPC) measurements were conducted in the Chemical Science and Engineering Division at Argonne National Laboratory (ANL) using a high-temperature GPC (Agilent-Polymer Laboratories 220) equipped with refractive index and viscometer detectors. Monodisperse polystyrene standards were used for calibration (ranging from 400 Da to 1.1 MDa). The column set included 3 Agilent PL-Gel Mixed B columns and 1 PL-Gel Mixed B guard column. 1,2,4-trichlorobenzene (TCB) containing 0.01 wt% 3,5-di-tert-butyl-4-hydroxytoluene (BHT) was chosen as the eluent with a flow rate of 1.0 mL/min at 150 °C. Samples were prepared in TCB at a concentration of ~1 – 2 mg/mL and heated at 130 °C for 24 h prior to injection.

^{13}C Cross Polarization/Magic Angle Spinning (CP/MAS) solid state nuclear magnetic resonance (NMR) spectroscopy was conducted at room temperature on a a Bruker Avance III 400 MHz spectrometer equipped with a 4mm HX probe. Sample data was acquired using TopSpin™ by Bruker. ^{13}C CP/MAS NMR data were collected using a spin rate of 10 KHz and a contact time (p15) of 5 ms at room temperature. D1 was set to 5.00 sec, SW was set to 296 ppm, and O1P was set to 100 ppm. 12,000 scans were used for ^{13}C CP/MAS NMR data collection. Samples were loaded neat into a 4 mm cylindrical zirconia rotor sealed with a Kel-F cap, both from Bruker. ^{13}C CP/MAS NMR spectra were referenced to an external adamantane peak at δ 38.3 and were converted to tetramethylsilane at δ 0.0. NMR spectra were reported after phase correction in MestReNova (MNova) by Mestrelab Research.

^1H and ^{13}C solution state NMR spectroscopy was conducted on a Bruker Avance III 600 MHz system equipped with two RF channels (^1H = 600 MHz, ^{13}C = 150 MHz). Sample data was acquired using TopSpin™ by Bruker. All collected spectra were referenced to residual solvent signals. NMR spectra were processed and integrated using Mnova by Mestrelab Research, following phase correction and baseline correction (Whittaker smoother). Initial ^1H solution state NMR spectra of the polymer product were collected in 1,1,2,2-tetrachloroethane-d_2 at 120 °C with 25 scans. D1 was set to 5.00 sec, SW was set to 16 ppm, and O1P was set to 6 ppm. Next, ^{13}C solution state NMR spectra of the polymer product were collected in 1,1,2,2-tetrachloroethane-d_2 at 120 °C with 18,000 scans. D1 was set to 2.00 sec, SW was set to 240 ppm, and O1P was set to 100 ppm. After ^{13}C solution state NMR data collection finished, final ^1H solution state NMR spectra of the polymer product were collected in 1,1,2,2-tetrachloroethane-d_2 at 120 °C with 25 scans. D1 was set to 5.00 sec, SW was set to 16 ppm, and O1P was set to 6 ppm. The polymer product was heated at 120 °C in 1,1,2,2-tetrachloroethane-d_2 prior to NMR data collection to aid in solubilization.

Differential scanning calorimetry (DSC) experiments were conducted using a Mettler Toledo TGA/DSC 1 LF and corresponding STARe software (v16.10). For DSC of polymers, samples were heated in 70 µL alumina crucibles under N_2 at 10 °C/min. from 25 °C to 200 °C and then cooled from 200 °C to 25 °C for two cycles.

Diffuse reflectance infrared Fourier transform spectroscopy (DRIFTS) experiments were conducted using a Thermo Scientific Nicolet iS50 FT-IR spectrometer equipped with an MCT-A detector cooled to 77 K. A Harrick Scientific Praying Mantis™ Diffuse Reflectance accessory was used to acquire spectra under air- and moisture-free conditions. Samples were prepared inside of a glovebox with argon atmosphere and DRIFTS spectra were collected under this atmosphere. KBr was used as a background for spectra. The collected spectra were processed using the Kubelka-Munk function.

X-ray photoelectron spectra were collected at the Keck-II/NUANCE facility at Northwestern University using a Thermo

Scientific ESCALAB 250Xi (Al Kα radiation, 1486.6 eV). All measurements were performed with an electron flood gun and were calibrated to C1s peak at 284.8 eV.

Results and discussion

Cr-SIM-NU-1000 was synthesized using a previously reported solvothermal deposition procedure with $CrCl_2$ as the Cr precursor.[50] Powder X-ray diffraction (PXRD) confirmed bulk phase purity, N_2 physisorption was performed to confirm porosity, and scanning electron microscopy (SEM) was used to confirm retention of crystallite morphology (**Figure 2**). Inductively coupled plasma-optical emission spectroscopy (ICP-OES) analysis revealed a Cr loading of 2.5 ± 0.3 Cr atoms per Zr_6 node or 5.4 ± 0.6 wt% Cr. These bulk characterizations confirm that framework integrity remains after the metalation step as reported previously,[50] and that remaining porosity can facilitate substrate diffusion to installed Cr sites and subsequent polymer formation.

With the addition of the DEAC co-catalyst necessary for catalytic activity at room temperature, as demonstrated previously,[50] the interactions between DEAC and the MOF catalyst were initially characterized using non-diffractive spectroscopic techniques. Specifically, X-ray photoelectron spectroscopy (XPS) and diffuse reflectance infrared Fourier transform spectroscopy (DRIFTS) were used to determine the electronic effect and potential interactions of DEAC with the node upon DEAC treatment at the same conditions as catalysis experiments (287:1 Al:Cr). Al 2p XPS (**Figure S5**) of DEAC and DEAC@Cr-SIM-NU-1000 exhibit nearly identical binding energies (75.3 and 75.2 eV) which are also 0.3 – 0.4 eV lower than other Al^{3+} salt standards, indicative of more electron rich Al species. Interestingly, looking into Cr 2p XPS (**Figure S6**) of the as synthesized catalyst and DEAC treated catalyst materials shows a lower binding energy in the DEAC treated material (577.2 eV) versus as synthesized (577.7 eV), suggesting a more electron rich Cr species after DEAC treatment. This lower binding energy is in alignment with the binding energy of the $CrCl_2$ precursor used to synthesize the catalyst material, suggesting an electrodeficient $Cr^{\delta+}$ active catalyst. Notably,

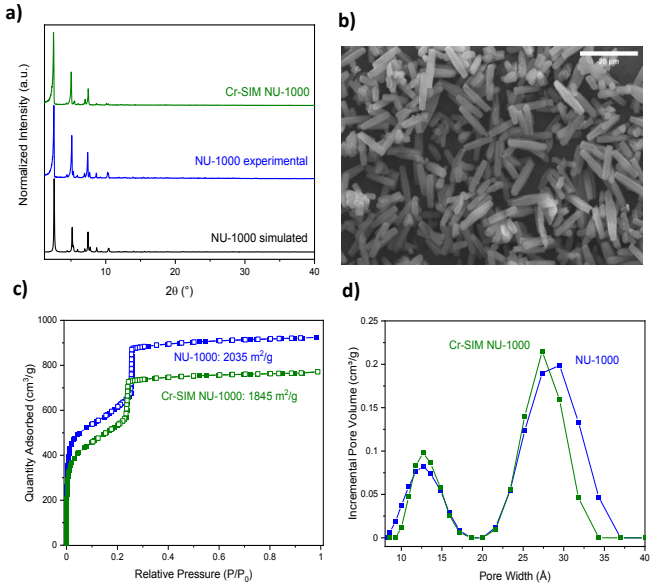

Figure 2. Bulk characterization of NU-1000 and Cr-SIM-NU-1000. a) powder X-ray diffraction patterns, b) SEM image of Cr-SIM-NU-1000 with scale bar 20 μm, c) N_2 isotherms at 77 K, and d) density functional theory computed pore size distributions.

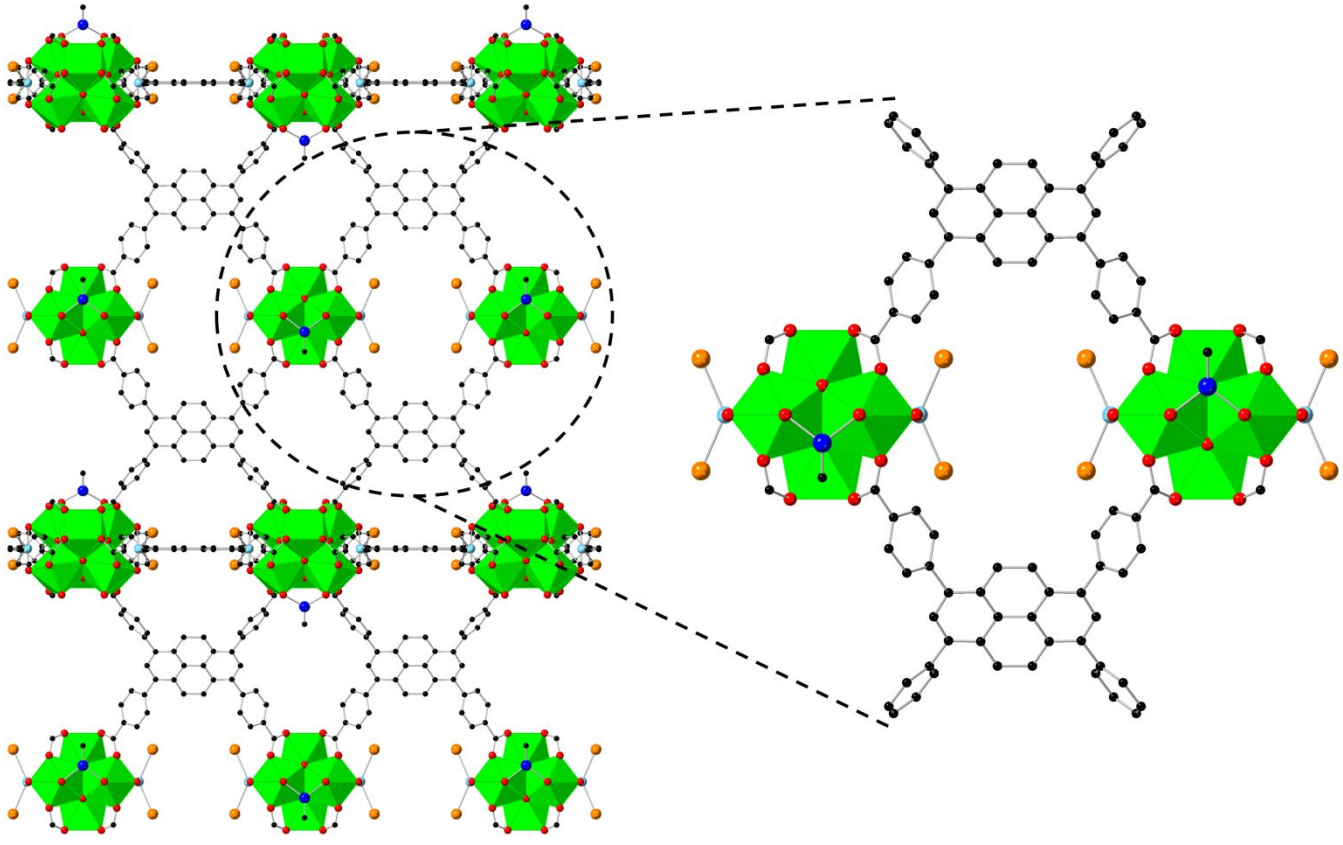

Figure 3. Experimental single crystal X-ray diffraction structure of DEAC@Cr-SIM-NU-1000. View of window between the nodes that occurs across the framework exhibiting occupation by DEAC sited at the oxy-ligands of the node (left). Zoomed in view of the c-pore showing crystallographically equivalent sites for both Cr (0.25 occupancy) and Al (right). Atom colors: carbon (gray), oxygen (red), aluminum (light blue), chlorine (orange), chromium (dark blue), zirconium (green). Hydrogen omitted for clarity.

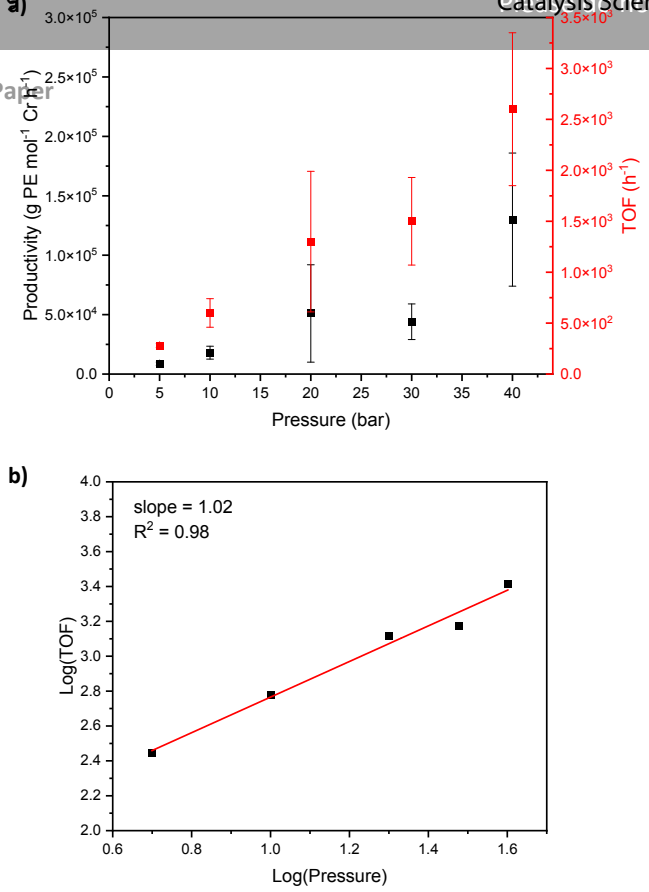

Figure 4. a) Plot of productivity and turnover frequency (TOF) of Cr-SIM-NU-1000 for ethylene polymerization vs. starting ethylene pressure. Error bars consist of five replicates. Reaction conditions: 0.006 mol% catalyst (10 mg), 1.0 mL 1.0 M Et_2AlCl in heptane (287 eq.), and 5 mL heptane in pressurized Parr vessel at room temperature with 200 rpm stirring for 1 hour. b) Log plot of TOF vs. C_2H_4 pressure.

there is also a slight increase in the Cr-O bond lengths in going from the as-synthesized catalyst to the DEAC treated material (**Table S5**). DRIFTS analysis of the as-synthesized catalyst and DEAC treated materials (**Figures S3 and S4**) show a loss of the remaining hydroxo peak (3690 cm^{-1}) in the Cr-SIM-NU-1000 spectrum after exposure to DEAC. This peak loss suggests that DEAC has interacted with the remaining hydroxo species through proton scavenging and/or node-grafting.

Taking the structural characterization a step further, single crystals of Cr-SIM-NU-1000 were treated with DEAC at the same exposure level as the catalysis experiments (287:1 Al:Cr), and subsequently characterized by SC-XRD. The species retains the *P6/mmm* space group and has very similar unit cell parameters to untreated Cr-SIM-NU-1000, with only a slight increase along *a* and *b* axes ($a = b = 39.433$ Å), and a slight decrease on the *c* axis ($c = 16.256$ Å). To confirm and quantify DEAC loading into the single crystal of the framework, we performed ICP-OES measurements on the treated single crystals. These measurements indicated DEAC loading at a level corresponding to 10 Al atoms per Zr_6 node. Additionally, the loss of the hydroxo peak in the DRIFT spectrum suggests that Al is depositing at the remaining terminal positions of the Zr_6 nodes located in the inter-node space (c-pore).

Notably, the atom bound to Cr is best assigned as carbon in the DEAC treated crystal structure, rather than the as synthesized Cl^- ligand, yielding a Cr-C bond of 1.59 Å, confirming the transfer of the ethyl group from DEAC to Cr. Additionally, the DEAC can be partially resolved in the crystal structure bound to terminal oxy-ligands at the node (**Figures 3 and S18**). Unfortunately, exposure to DEAC degraded the crystals, and only the first C of the Cr-ethyl, and the Al and Cl of node deposited DEAC, were visible in the structure. However, all resolved Al atoms sit within the window, or c-pore, of the framework at the terminal hydroxyl and aqua groups of the Zr_6 node; Cr sits at 6.00 Å from the resolved Al atoms, and as such continuing interactions between Al and Cr are unlikely, since an Al-Cr coordination bond of this length is unrealistic. No substantial residual electron density can be seen in the hexagonal or triangular pores (**Figure S19**), but in addition to the resolved Al atoms at the node there is still some residual unassigned electron density located within the c-pore (**Figure S20**). This residual electron density is likely more DEAC sited within the pore but not coordinated to the Zr_6 node. Large distances between trivalent metal chlorides and Zr nodes have been previously seen in MOFs,[52] and DEAC dimers are reasonably stable at room temperature against dissociation to the monomeric species.[53-55] As has been shown with other alkyl aluminum species,[53] diethylaluminum chloride (DEAC) exists as a dimer in solution at room temperature. The co-catalyst solution used for these studies is 1.0 M DEAC in heptane with catalyst treatment using DEAC always occurring at room temperature. Thus, while crystallographically resolved as coordinating to the node, we propose that DEAC also inhabits the window pore as a dimer when it no longer has surface hydroxo or aqua ligands with which to react. To our knowledge, this represents the first crystallographic study to identify a Cr-C bond after DEAC treatment of a heterogeneous catalyst/porous support and resolve the DEAC co-catalyst, at least partially, within such a system.

To test the activity of Cr-SIM-NU-1000 for ethylene polymerization, the catalyst was evaluated in a Parr pressure vessel over a range of ethylene pressures. To perform these reactions, the vessel was charged with catalyst, DEAC co-catalyst (287:1 Al:Cr), and 5 mL heptane in an Ar-filled glovebox before being pressurized to between 5 and 40 bar with ethylene. The reactor was then left at room temperature for 1 hour, before the reaction was quenched and the polymer and catalyst were collected on the benchtop. Polymer yield was determined by isolated mass. As ethylene pressure was increased, the average turnover frequency as well as productivity metric (g PE mol^{-1} Cr h^{-1}) showed an apparent increasing trend, reaching the highest activity at 40 bar ethylene with a turnover frequency of 2.6×10^3 h^{-1} and polyethylene productivity of 1.3×10^5 g PE mol^{-1} Cr h^{-1} (**Figure 4a**). In fact, plotting log(TOF) vs. log(C_2H_4 pressure) yields a slope of ~ 1 (**Figure 4b**), evidence of a linear dependence of turnover frequency on ethylene pressure and evidence against intrapore condensation of ethylene seen in other MOF materials.[37, 56, 57]

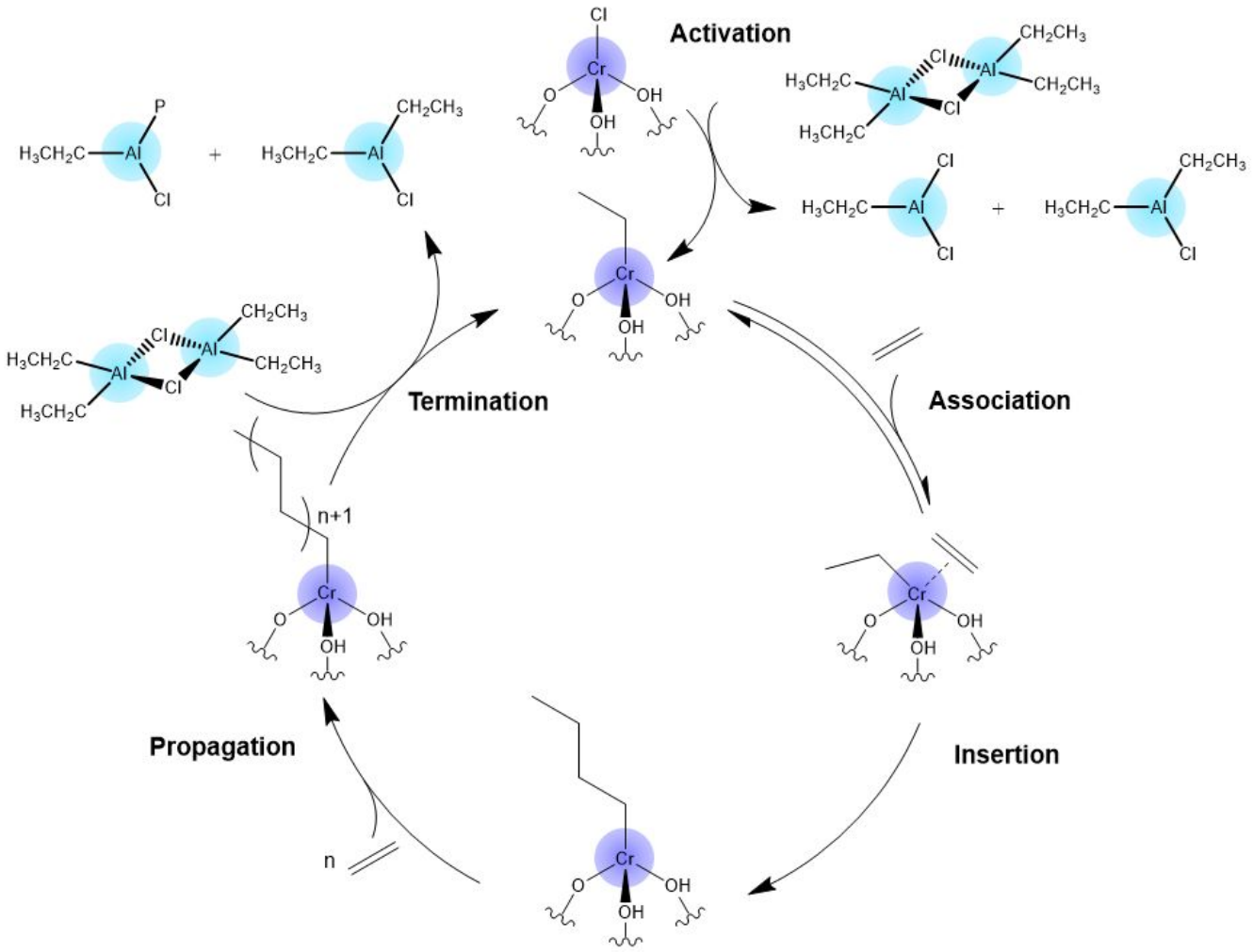

Figure 5. Proposed mechanism of ethylene polymerization using Cr-SIM-NU-1000 as the catalyst and diethyl aluminum chloride as the activator and chain termination agent. Cr-SIM-NU-1000 is first activated by DEAC to provide Cr-ethyl which allows subsequent chain growth through linear insertion of ethylene into the Cr-alkyl bond. Chain termination occurs through transfer to DEAC. P = polymer chain.

Polymer samples produced by Cr-SIM-NU-1000 can be described as linear polyethylene as evidenced by a single peak, assignable to the polymer, and lack of branched peaks observed in the solid-state ^{13}C CP/MAS NMR (**Figure S13**)[58-61] and solution ^{13}C NMR (**Figure S16**) spectra. Heat of fusion calculations from DSC measurements[62] (**Table S2**) further indicate that the polymer produced is high-density, having an average melting temperature of 137 °C and 42% crystallinity. GPC analysis revealed that the polymer produced has an average molecular weight that depends on the initial pressure of ethylene. In general, with increasing ethylene pressure, the molecular weight of the polymers increased while the polydispersity decreased, reaching a weight average molecular weight (M_w) of 920 kDa with a polydispersity of 2.0 (see **Table S3**). It is important to note that prior to GPC analysis, the catalyst was removed (by filtration) as a necessary step during sample preparation. Conceivably, MOF removal could have resulted in the removal of ultra-high molecular weight polymer and polymer trapped within the pores of the framework. Extensive washing of the post-catalysis material (MOF and polymer) leads to substantial removal of surface polymer (**Figures S9-S12**);[63-65] however, complete removal of polymer from the framework was not achieved. Nonetheless, it remains that Cr-SIM-NU-1000 is a competent catalyst for ethylene polymerization, with a uniformly active single site as indicated by the low polydispersity generally seen with other single-site catalysts such as metallocenes.[2]

Furthermore, given the defined structure of the MOF and supported catalyst, connections can be drawn to the polymer properties and a mechanism can be proposed (**Figure 5**). Supported Cr-based ethylene polymerization catalysts have been proposed to proceed through Cossee-Arlman (linear insertion) and metallacycle chain growth mechanisms, and can subsequently terminate through a variety of methods including β-H elimination to the metal, β -H transfer to the monomer, or chain transfer to aluminum.[66, 67] With Cr-SIM-NU-1000, given the lack of activity without addition of DEAC, the alkyl aluminum co-catalyst serves to activate the Cr species within the MOF by providing an initial ethyl group and generating an alkyl-Cr species. This activation by alkylation is supported by the Cr-C bond resolved in the crystal structure of DEAC@Cr-SIM-NU-1000. Next, after ethylene coordination to the Cr, or in a concerted manner, linear insertion (Cossee-Arlman) of ethylene occurs. Linear insertion is the most likely mechanism since substantial α-olefin production, rather than polymer, is expected for the metallacycle mechanism.[68] The geometry of the framework support, namely the 1-dimensional channels of the **csq** topology that NU-1000 exhibits,[51]

is likely to facilitate the linear insertion chain growth mechanism, noting that the Cr species exclusively faces into the hexagonal 3 nm mesopore, as shown in **Figure 1**. Based on solution ^{1}H NMR spectra of the polyethylene product (**Figures S15 and S17**), the absence of olefinic signals indicates that the termination step of the polymerization is exclusively chain transfer to aluminum species, as seen by other ethylene polymerization systems activated by DEAC.[69] In addition, chain walking – and subsequent branching – is not observed in this system by ^{13}C NMR (**Figure S16**), an important component to be expected in the β-hydrogen elimination pathway, more commonly seen with late transition metal catalysts.[68]

Conclusions

Cr-SIM-NU-1000 serves as a structurally well-defined Cr-based ethylene polymerization catalyst that offers insight into the inner workings of similar heterogeneous catalysts unable to be characterized crystallographically. While this report resolves the Cr-C bond and the approximate crystallographic location of the DEAC within a heterogeneous ethylene polymerization catalyst structure, it should be acknowledged that this is a pre-catalyst structure, and not the *operando* catalyst structure. By collecting diffraction data that leads to structural elucidation of the pre-catalyst material, this MOF-supported catalyst shows the potential for improving upon our understanding of heterogeneous polymerization systems. With that in mind, we are able to provide a proposed mechanism for this catalyst and co-catalyst system, wherein the polymerization proceeds through a linear insertion chain growth and terminates *via* chain transfer to the alkyl aluminum co-catalyst. There is still more to be done to fully elucidate the mechanism and influence of co-catalyst concentrations or identity on the resulting activity of this system and polymer produced. Subsequent work looking at *in-situ* crystallographic and spectroscopic techniques can aid in the determination of the oxidation state and potential structural changes of the catalyst during the process of the reaction, something unable to be obtained without the structural definition of this uniformly supported catalyst. Efforts to this end are ongoing in our laboratories.

Conflicts of interest

O.K.F. and J.T.H. have financial interests in NuMat Technologies, a company that commercializes MOFs.

Acknowledgements

This work was supported as part of the Inorganometallic Catalyst Design Center, an Energy Frontiers Research Center (EFRC) funded by the Department of Energy (DOE), Office of Science, Basic Energy Sciences under award number DE-SC0012702. This work made use of the IMSERC X-ray facility at Northwestern University, which has received support from the Soft and Hybrid Nanotechnology Experimental (SHyNE) Resource (NSF ECCS-1542205), and Northwestern University. This work also made use of the EPIC facility of Northwestern University's NUANCE Center, which has received support from the SHyNE Resource (NSF ECCS-1542205), the International Institute of Nanotechnology, and Northwestern's MRSEC program (NSF DMR-1720139). This work made use of the IMSERC NMR facility at Northwestern University, which has received support from the Soft and Hybrid Nanotechnology Experimental (SHyNE) Resource (NSF ECCS-2025633), International Institute of Nanotechnology, and Northwestern University. J.G.K. and Z.H.S. were supported by the National Science Foundation (NSF) Graduate Research Fellowship under Grant No. (DGE-1842165). The authors thank Florencia A. Son for collecting SEM images and Dr. Yuyang Wu for assistance in NMR data analysis and helpful discussions. The authors also thank Prof. Neil Schweitzer for facilitating instrument use in the Reactor Engineering and Catalyst Testing (REACT) core facility and for helpful discussions.

Abbreviations

CP/MAS, cross polarization/magic angle spinning; DEAC, diethylaluminum chloride; DEF, *N,N*-diethylformamide; DFT, density functional theory; DMF, *N,N*-dimethylformamide; DSC, differential scanning calorimetry; GPC, gel permeation chromatography; ICP-OES, inductively coupled plasma – optical emission spectroscopy; MOF, metal–organic framework; NMR, nuclear magnetic resonance; NU, Northwestern University; PE, polyethylene; PXRD, powder X-ray diffraction; SC-XRD, single crystal X-ray diffraction; SEM, scanning electron microscopy; SIM, solvothermal deposition in MOFs; $TBAPy^{4-}$, 1,3,6,8-tetrakis(p-benzoate)pyrene; XPS, X-ray photoelectron spectroscopy.

References

1. L. A. Utracki, *Polymer Engineering & Science*, 1995, **35**, 2-17.
2. M. P. McDaniel, *A Review of the Phillips Supported Chromium Catalyst and Its Commercial Use for Ethylene Polymerization*, Elsevier Inc., 1 edn., 2010.
3. C. M. Friend and B. Xu, *Acc Chem Res*, 2017, **50**, 517-521.
4. C. Brown, A. Lita, Y. Tao, N. Peek, M. Crosswhite, M. Mileham, J. Krzystek, R. Achey, R. Fu, J. K. Bindra, M. Polinski, Y. Wang, L. J. van de Burgt, D. Jeffcoat, S. Profeta, A. E. Stiegman and S. L. Scott, *ACS Catalysis*, 2017, **7**, 7442-7455.
5. A. Zecchina and E. Groppo, *Proceedings of the Royal Society A: Mathematical, Physical and Engineering Sciences*, 2012, **468**, 2087-2098.
6. E. Groppo, G. A. Martino, A. Piovano and C. Barzan, *ACS Catalysis*, 2018, **8**, 10846-10863.
7. E. Morra, G. A. Martino, A. Piovano, C. Barzan, E. Groppo and M. Chiesa, *The Journal of Physical Chemistry C*, 2018, **122**, 21531-21536.
8. M. P. McDaniel, *Industrial & Engineering Chemistry Research*, 2002, **27**, 1559-1564.
9. T. W. van Deelen, C. Hernández Mejía and K. P. de Jong, *Nature Catalysis*, 2019, **2**, 955-970.
10. H. C. Zhou, J. R. Long and O. M. Yaghi, *Chemical Reviews*, 2012, **112**, 673-674.
11. L. Feng, G. S. Day, K.-Y. Wang, S. Yuan and H.-C. Zhou, *Chem*, 2020, **6**, 2902-2923.
12. A. J. Howarth, Y. Liu, P. Li, Z. Li, T. C. Wang, J. T. Hupp and O. K. Farha, *Nature Reviews Materials*, 2016, **1**, 1-15.
13. T. Islamoglu, S. Goswami, Z. Li, A. J. Howarth, O. K. Farha and J. T. Hupp, *Accounts of Chemical Research*, 2017, **50**, 805-813.

14. Z. Wang and S. M. Cohen, *Chem Soc Rev*, 2009, **38**, 1315-1329.
15. Y. F. Song and L. Cronin, *Angew Chem Int Ed Engl*, 2008, **47**, 4635-4637.
16. A. Kirchon, L. Feng, H. F. Drake, E. A. Joseph and H. C. Zhou, *Chemical Society Reviews*, 2018, **47**, 8611-8638.
17. H. Furukawa, K. E. Cordova, M. O'Keeffe and O. M. Yaghi, *Science*, 2013, **341**, 1230444.
18. R.-B. Lin, S. Xiang, H. Xing, W. Zhou and B. Chen, *Coordination Chemistry Reviews*, 2019, **378**, 87-103.
19. H. Li, L. Li, R.-B. Lin, W. Zhou, Z. Zhang, S. Xiang and B. Chen, *EnergyChem*, 2019, **1**.
20. H. Li, K. Wang, Y. Sun, C. T. Lollar, J. Li and H. C. Zhou, *Materials Today*, 2018, **21**, 108-121.
21. W.-T. Koo, J.-S. Jang and I.-D. Kim, *Chem*, 2019, **5**, 1938-1963.
22. Y. Zhang, S. Yuan, G. Day, X. Wang, X. Yang and H. C. Zhou, *Coordination Chemistry Reviews*, 2018, **354**, 28-45.
23. R. J. Drout, L. Robison, Z. Chen, T. Islamoglu and O. K. Farha, *Trends in Chemistry*, 2019, **1**, 304-317.
24. E. M. Dias and C. Petit, *Journal of Materials Chemistry A*, 2015, **3**, 22484-22506.
25. F. Carraro, K. Chapman, Z. Chen, M. Dincă, T. Easun, M. Eddaoudi, O. Farha, R. Forgan, L. Gagliardi, F. Haase, D. Harris, S. Kitagawa, J. Knichal, C. Lamberti, J. S. M. Lee, K. Leus, J. Li, W. Lin, G. Lloyd, J. R. Long, C. Lu, S. Ma, L. McHugh, J. P. H. Perez, M. Ranocchiari, N. Rosi, M. Rosseinsky, M. R. Ryder, V. Ting, M. Van Der Veen, P. Van Der Voort, D. Volkmer, A. Walsh, D. Woods and O. M. Yaghi, *Faraday Discussions*, 2017, **201**, 369-394.
26. C. Wang, B. An and W. Lin, *ACS Catalysis*, 2018, **9**, 130-146.
27. D. Yang and B. C. Gates, *ACS Catalysis*, 2019, **9**, 1779-1798.
28. M. Rimoldi, A. J. Howarth, M. R. DeStefano, L. Lin, S. Goswami, P. Li, J. T. Hupp and O. K. Farha, *ACS Catalysis*, 2016, **7**, 997-1014.
29. T. Drake, P. Ji and W. Lin, *Acc Chem Res*, 2018, **51**, 2129-2138.
30. F. Ren and P. Ji, *Catalysts*, 2020, **10**.
31. K. O. Kirlikovali, Z. Chen, T. Islamoglu, J. T. Hupp and O. K. Farha, *ACS Appl Mater Interfaces*, 2020, **12**, 14702-14720.
32. Y. Liu, A. J. Howarth, N. A. Vermeulen, S. Y. Moon, J. T. Hupp and O. K. Farha, *Coordination Chemistry Reviews*, 2017, **346**, 101-111.
33. M. C. de Koning, M. van Grol and T. Breijaert, *Inorg Chem*, 2017, **56**, 11804-11809.
34. Z. H. Syed, Z. Chen, K. B. Idrees, T. A. Goetjen, E. C. Wegener, X. Zhang, K. W. Chapman, D. M. Kaphan, M. Delferro and O. K. Farha, *Organometallics*, 2020, **39**, 1123-1133.
35. X. Feng, Y. Song, Z. Li, M. Kaufmann, Y. Pi, J. S. Chen, Z. Xu, Z. Li, C. Wang and W. Lin, *J Am Chem Soc*, 2019, **141**, 11196-11203.
36. T. A. Goetjen, J. Liu, Y. Wu, J. Sui, X. Zhang, J. T. Hupp and O. K. Farha, *Chem Commun (Camb)*, 2020, **56**, 10409-10418.
37. H. D. Park, R. J. Comito, Z. Wu, G. Zhang, N. Ricke, C. Sun, T. Van Voorhis, J. T. Miller, Y. Román-Leshkov and M. Dincă, *ACS Catalysis*, 2020, **10**, 3864-3870.
38. M. K. Jongkind, M. Rivera-Torrente, N. Nikolopoulos and B. M. Weckhuysen, *Chemistry*, 2021, **27**, 5769-5781.
39. K.-i. Otake, J. Ye, M. Mandal, T. Islamoglu, C. T. Buru, J. T. Hupp, M. Delferro, D. G. Truhlar, C. J. Cramer and O. K. Farha, *ACS Catalysis*, 2019, **9**, 5383-5390.
40. J. Liu, J. Ye, Z. Li, K. I. Otake, Y. Liao, A. W. Peters, H. Noh, D. G. Truhlar, L. Gagliardi, C. J. Cramer, O. K. Farha and J. T. Hupp, *J Am Chem Soc*, 2018, **140**, 11174-11178.
41. X. Wang, X. Zhang, P. Li, K. I. Otake, Y. Cui, J. Lyu, M. D. Krzyaniak, Y. Zhang, Z. Li, J. Liu, C. T. Buru, T. Islamoglu, M. R. Wasielewski, Z. Li and O. K. Farha, *Journal of the American Chemical Society*, 2020, **141**, 8306-8314.
42. Y. Yang, X. Zhang, S. Kanchanakungwankul, Z. Lu, H. Noh, Z. H. Syed, O. K. Farha, D. G. Truhlar and J. T. Hupp, *J Am Chem Soc*, 2020, **142**, 21169-21177.
43. Y. Chen, X. Zhang, X. Wang, R. J. Drout, M. R. Mian, R. Cao, K. Ma, Q. Xia, Z. Li and O. K. Farha, *J Am Chem Soc*, 2021, **143**, 4302-4310.
44. G. Zhou, B. Wang and R. Cao, *J Am Chem Soc*, 2020, **142**, 14848-14853.
45. K. I. Otake, Y. Cui, C. T. Buru, Z. Li, J. T. Hupp and O. K. Farha, *J Am Chem Soc*, 2018, **140**, 8652-8656.
46. Z. H. Syed, F. Sha, X. Zhang, D. M. Kaphan, M. Delferro and O. K. Farha, *ACS Catalysis*, 2020, **10**, 11556-11566.
47. M. C. Wasson, C. T. Buru, Z. Chen, T. Islamoglu and O. K. Farha, *Applied Catalysis A: General*, 2019, **586**, 117214-117214.
48. T. C. Wang, N. A. Vermeulen, I. S. Kim, A. B. Martinson, J. F. Stoddart, J. T. Hupp and O. K. Farha, *Nat Protoc*, 2016, **11**, 149-162.
49. J. E. Mondloch, W. Bury, D. Fairen-Jimenez, S. Kwon, E. J. DeMarco, M. H. Weston, A. A. Sarjeant, S. T. Nguyen, P. C. Stair, R. Q. Snurr, O. K. Farha and J. T. Hupp, *J Am Chem Soc*, 2013, **135**, 10294-10297.
50. T. A. Goetjen, X. Zhang, J. Liu, J. T. Hupp and O. K. Farha, *ACS Sustainable Chemistry and Engineering*, 2019, **7**, 2553-2557.
51. T. Islamoglu, K.-i. Otake, P. Li, C. T. Buru, A. W. Peters, I. Akpinar, S. J. Garibay and O. K. Farha, *CrystEngComm*, 2018, **20**, 5913-5918.
52. K. I. Otake, S. Ahn, J. Knapp, J. T. Hupp, J. M. Notestein and O. K. Farha, *Inorg Chem*, 2021, **60**, 2457-2463.
53. J. P. Blitz, R. E. Diebel, C. A. Deakyne, J. M. Christensen and V. M. Gun'ko, *J Phys Chem B*, 2005, **109**, 5667-5677.
54. B. t. Champagne, D. H. Mosley, J. G. Fripiat, A. Jean-Marie, A. Bernard, S. Bettonville, P. François and A. Momtaz, *Journal of Molecular Structure: THEOCHEM*, 1998, **454**, 149-159.
55. R. Rottler, C. G. Kreiter and G. Fink, *Zeitschrift für Naturforschung B*, 1976, **31**, 730-736.
56. I. Agirrezabal-Telleria, I. Luz, M. A. Ortuno, M. Oregui-Bengoechea, I. Gandarias, N. Lopez, M. A. Lail and M. Soukri, *Nat Commun*, 2019, **10**, 2076.
57. I. Agirrezabal-Telleria and E. Iglesia, *Journal of Catalysis*, 2017, **352**, 505-514.
58. M. Pollard, K. Klimke, R. Graf, H. W. Spiess, M. Wilhelm, O. Sperber, C. Piel and W. Kaminsky, *Macromolecules*, 2004, **37**, 813-825.
59. A. Kaji, A. Yamanaka and M. Murano, *Polymer Journal*, 1990, **22**, 893-900.
60. A. Tapash, P. J. DesLauriers and J. L. White, *Macromolecules*, 2015, **48**, 3040-3048.
61. W. L. Jarrett, L. J. Mathias and R. S. Porter, *Macromolecules*, 2002, **23**, 5164-5166.

62. F. M. Mirabella and A. Bafna, *Journal of Polymer Science Part B: Polymer Physics*, 2002, **40**, 1637-1643.
63. M. F. Bergstra and G. Weickert, *Macromolecular Materials and Engineering*, 2005, **290**, 610-620.
64. I. Kim, J. H. Kim and S. I. Woo, *Journal of Applied Polymer Science*, 1990, **39**, 837-854.
65. D. P. Gates, S. A. Svejda, E. Oñate, C. M. Killian, L. K. Johnson, P. S. White and M. Brookhart, *Macromolecules*, 2000, **33**, 2320-2334.
66. A. Fong, Y. Yuan, S. L. Ivry, S. L. Scott and B. Peters, *ACS Catalysis*, 2015, **5**, 3360-3374.
67. D. S. McGuinness, *Chem Rev*, 2011, **111**, 2321-2341.
68. P. H. M. Budzelaar, *Wiley Interdisciplinary Reviews: Computational Molecular Science*, 2012, **2**, 221-241.
69. M. Białek, *Journal of Polymer Science Part A: Polymer Chemistry*, 2010, **48**, 3209-3214.